Additive Manufacturing 16 (2017) 98–106

Contents lists available at ScienceDirect

Additive Manufacturing

journal homepage: www.elsevier.com/locate/addma

Full length article

Design framework for multifunctional additive manufacturing: Coupled optimization strategy for structures with embedded functional systems

Ajit Panesar*, Ian Ashcroft, David Brackett, Ricky Wildman, Richard Hague

Faculty of Engineering,University Park, University of Nottingham, NG7 2RD, UK

ARTICLE INFO

Article history:
Received 4 November 2016
Received in revised form 24 February 2017
Accepted 21 May 2017
Available online 23 May 2017

Keywords:
Optimization
Additive manufacturing
Multi-functional
Computational methods

ABSTRACT

The driver for this research is the development of multi-material additive manufacturing processes that provide the potential for multi-functional parts to be manufactured in a single operation. In order to exploit the potential benefits of this emergent technology, new design, analysis and optimization methods are needed. This paper presents a method that enables in the optimization of a multifunctional part by coupling both the system and structural design aspects. This is achieved by incorporating the effects of a system, comprised of a number of connected functional components, on the structural response of a part within a structural topology optimization procedure. The potential of the proposed method is demonstrated by performing a coupled optimization on a cantilever plate with integrated components and circuitry. The results demonstrate that the method is capable of designing an optimized multifunctional part in which both the structural and system requirements are considered.

1. Introduction

Single-material additive manufacturing (AM) processes, such as selective laser melting, enable the design of geometrically complex parts. Multimaterial additive manufacturing (MMAM) further expands this design freedom to include the spatial variation of material composition and enable multifunctionality through the volume of a part. Multifunctionality, by definition, necessitates the embedding of active sub-components in order to deliver additional functional capability, such as electronic, electro-mechanical, optical, electromagnetic, chemical and thermal [1]. MacDonald and Wicker [1], in a recent review article, identified multifunctional additive manufacturing (MFAM) as a pivotal technology in advancing the future of AM. Efforts have been made by researchers to develop hybrid systems to achieve MFAM, one such example is the work by Lopes et al. [2] where stereolithography and direct print technologies are combined to realize additively manufactured electronic devices. Such hybrid approaches often require multiple machine/print-restarts and additional manual or automated accompanying procedures. Conversely, multi-head inkjet printing, a promising MMAM process allows for MFAM designs to be realized with greater degree of manufacturing freedom in a single operation by co-depositing structural and functional inks. Recent works [3–5] have demonstrated the potential of jetting for electronics applications and highlighted the considerable ongoing research into materials and process development for MMAM.

Steps towards exploiting the design freedoms of AM have also been made. OpenFab [6] defined a procedure to efficiently grade mechanical properties through the volume of a part and Ponche et al. [7] proposed a three step global design approach with the aim of better integration of the design requirements (functional specification) with the AM process. However, there has been little work carried out to date on developing the design philosophies to realize novel MFAM concepts. The authors consider a closer interplay between the MMAM and topology optimization (TO – a structural optimization technique that iteratively improves the material layout within a given design space, for a given set of loads and boundary conditions [8]) key to progressing the MFAM design paradigm. One direct beneficiary of this is the area of 3D printed electronics, as fabrication of rugged structures that embed non-traditional electronic systems in an arbitrary form become possible [2,9]. This approach has the potential to pave the way for lightweight, more compact, better integrated and more optimal designs.

TO with embedded components has been investigated previously for the "integrated layout design" problem [10–13], where the aim has been to find both the optimal placement and orientation of components and the optimal configuration of the material simultaneously. This was achieved by iteratively changing the geo-

* Corresponding author.
E-mail address: ajit.panesar@gmail.com (A. Panesar).

http://dx.doi.org/10.1016/j.addma.2017.05.009

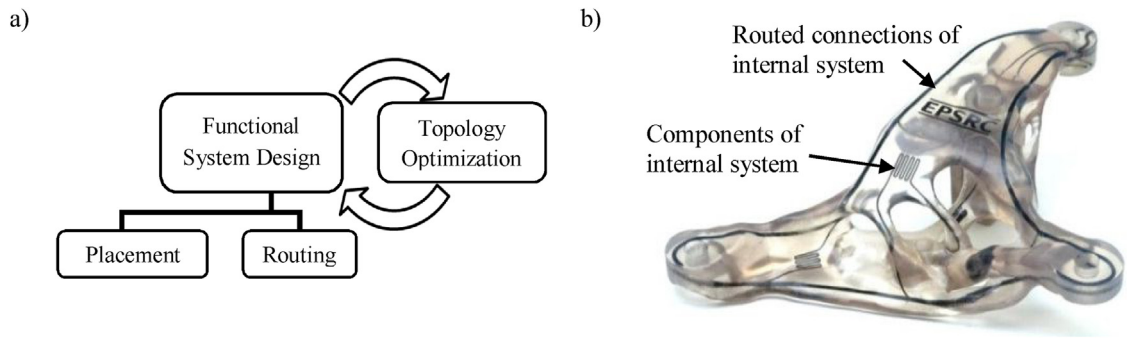

Fig. 1. Multifunctional design – a) top-level diagram showing coupled optimization of structures with embedded system, b) multi-material jetted concept prototype showing an optimized structural part that embeds an internal system (comprised of placed components and the associated routing) intended for the purpose of structural health monitoring.

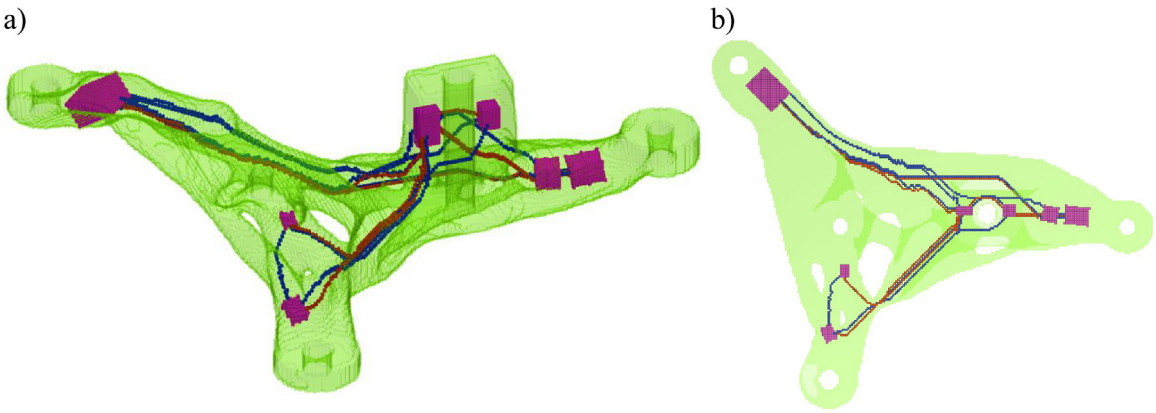

Fig. 2. Example of a TO automotive component (transmission mount) with embedded systems – demonstrating 3D placement of components and associated routing a) perspective view, b) top view.

metrical design variables describing the location and orientation of components within a TO regime. In all the reported instances, the implementation remained limited to the inclusion of rigid components that solely intended to enhance the structural performance. Therefore, this works seeks to make a step forward towards the inclusion of functional components (or a system) in a structure enabling the optimization of a MFAM design. To realize this aim, i.e. optimize the design of a multifunctional part, coupling both the system design (which is based on a functional performance i.e. not limited to only capturing structural or mechanical behaviour) and structural design, as illustrated in Fig. 1, is needed.

Earlier work by the authors detailed a MFAM design framework [9] to realize a functional system, specifically aimed at 3D Printed Circuit Volume (PCV) applications i.e. printed electronics in true 3D – not limited to, for example, printing on surfaces as in [2] or the stacked 2D (i.e. 2.5D) Printed Circuit Board (PCB) paradigm [14]. This work presented methods for the intelligent placement of functional components at suitable sites, and the associated routing for the conductive pathways within a part manufactured using multi-material jetting. Moreover, efforts were made to integrate these aspects of system design into a TO procedure such that the finite element analysis (FEA) conducted as part of a TO accounted for the updated material properties, reflecting system attributes [15]. Subsequently, this was extended to benefit from a bi-directional coupling between the TO and system design but the implementation remained limited to a specific routing method and suffered from robustness issues [16].

The capability for designing MFAM concepts for PCV application is in its infancy and therefore this work focuses on developing a generic coupled optimization strategy for the realisation of structures with embedded functional systems that are intended for manufacture using multi-material jetting. The paper takes the following structure: firstly, a description of design for functional systems is provided; secondly, the structure-system coupling strategy is presented; thirdly, the heuristic definition of the system sensitivities is detailed (so that one can tackle a bi-directional structure-system coupling); and lastly, the appropriateness and robustness of this strategy is demonstrated by evaluating and discussing the results for example test cases.

2. Methodology

A voxel modeling environment is chosen for seamless transition between system design, numerical analysis and manufacture as they all rely on discretized volumetric space [9]. Specifically, voxels for system design, hexahedral elements for FEA and 2D pixels with associated layer thickness in the raster-based (bmp) file format employed in jetting. Adoption of the voxel modeling environment eliminates the need for manual computer-aided-design operations, including conversion to the common STereoLithography file format and associated slicing, which is well known to be cumbersome and error prone.

2.1. Functional system design

The key enablers for making the functional system design possible are: (i) intelligent component placement and (ii) the associated connections routed between them. For simplicity, these are referred to as placement and routing. Although advancements in PCB design has led to the development of several graph algorithms

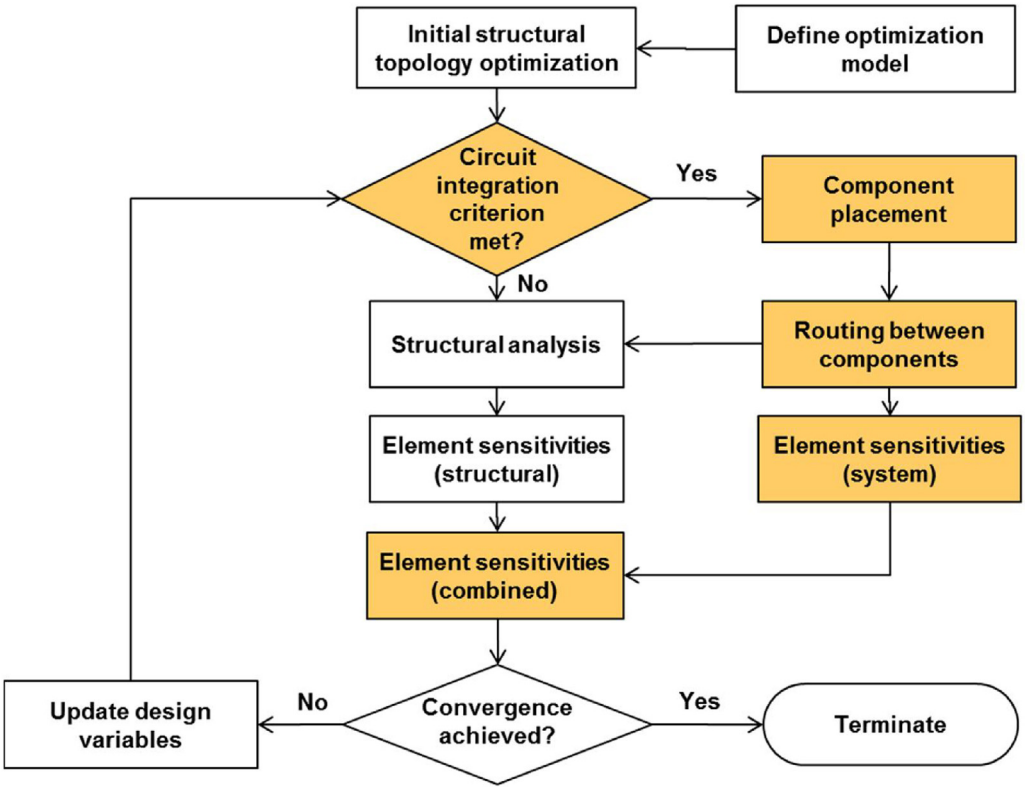

Fig. 3. Flowchart showing the coupled optimization procedure.

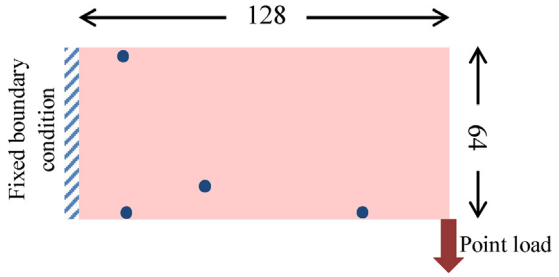

Fig. 4. The 2D cantilever problem with functional sites to be connected to form the system indicated by circles.

and mathematical methods, as reported in [17–19], the implementations have been, at best, geared at the 2.5D paradigm. Many of the PCB design strategies have been adapted and coupled with global evolutionary optimization algorithms to solve optimization problems in other fields. Examples include, Genetic Algorithms (GA) and Ant Colony Optimization (ACO), employed for pipe/cable routing problems [20–23] and optimum placement problems in structural health monitoring applications [24,25].

To successfully realize structures with embedded functional systems, one needs to explore the true 3D design freedoms offered by MFAM in an automated sense and earlier work by the authors [9] discusses how this can be achieved. The key elements of the proposed methods and their foundational principles are summarised below:

i. the intelligent placement of components – location selection based on a performance and/or geometry criterion; component orientation identified using skeletal information. The skeletal information (or the 1D medial axis) of a part's topology is obtained using a thinning algorithm, as detailed in [26,27].

ii. the generation of connections to form a circuit, i.e. routing – two approaches proposed to achieve this are: i) approximate routing which employs Dijkstra's algorithm [28] to find the shortest path on a 1D medial axis (i.e. skeletal) graph, ii) accurate routing which uses an implementation of the Fast Marching (FM) method [29].

Fig. 2 shows an example capturing the functional system design capability in 3D. Here, the high level of accuracy achieved using the FM implementation for identifying the shortest routes between a set of components that are not limited to planar orientation constraints (as is the case with 2.5D PCB paradigm) is demonstrated.

In principle, it is best to perform routing and placement concurrently but as they have nested dependencies, realizing a solution to a practical problem may become unviable. Therefore these two steps are often tackled independently. With regards to the system design considered here, placement of a component is kept fixed and the method of accurate routing is implemented. The system optimization problem therefore becomes a routing optimization problem with the aim is to improve the circuit efficiency by lowering energy losses, which are proportional to the resistance. This is achieved by identifying the shortest paths between components (as resistance is proportional to the path length) subject to various design rules and constraints. By doing so, we also minimise the utilization of the expensive material used for conductive tracks, providing further economic benefit.

2.2. Coupling strategy

Notable TO methods, such as SIMP [8], BESO [30] and level-set [31], have been principally developed to identify the stiffest structure (through compliance minimization) for a given mass constraint, and though their implementations have been demonstrated for other applied problems [32,33], most benchmark studies con-

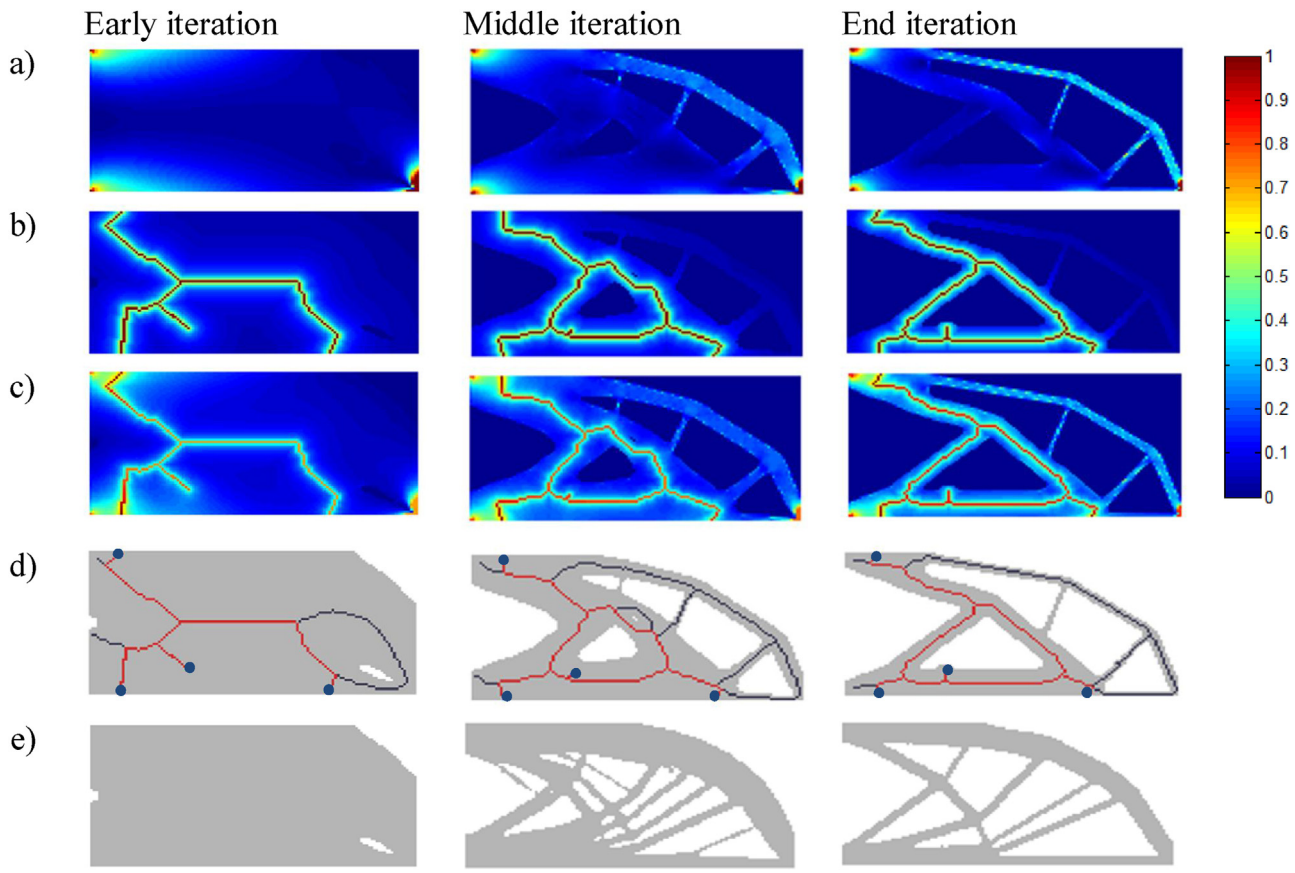

Fig. 5. Effects of system integration included in the process of structural topology optimization – a) Sensitivities for structure, b) sensitivities for internal system, c) combined sensitivities, d) resulting coupled solution, and e) TO using just structural sensitivities for comparison.

sider a classic cantilever plate or beam problem and therefore this work also utilizes such a structure to investigate the proposed coupling strategy.

Both BESO and level-set implementations reveal a well-defined boundary at every iteration of the optimization process, allowing for embedded system realisation (as discussed in [9]). However, it is only the former that provides the structural elemental sensitivity within the volume of the boundary enabling the optimization procedure of Fig. 3 to combine this with the corresponding system sensitivities to govern the evolution of the combined (structure + system) solution. In this paper the TO procedure (indicated in Fig. 3) is based on the revised BESO method [30,34,35] or what one might call the discrete SIMP method [36].

The compliance (a measure of the inverse of stiffness) based on a purely structural optimization problem can be stated as minimise:

$$\boldsymbol{C} = \frac{1}{2}\boldsymbol{U}^{\boldsymbol{T}}\boldsymbol{K}\boldsymbol{U} \tag{1}$$

subject to:

$$\boldsymbol{V_f} - \sum_{\boldsymbol{i}=1}^{\boldsymbol{N}} \boldsymbol{V_i}\boldsymbol{x_i} = 0 \tag{2}$$

where C is the total strain energy (commonly termed compliance), K is the global stiffness matrix and U is the global displacement vector, V_i is the elemental volume fraction, V_f is the structural target volume fraction constraint, and $x_i = x_{\min}$ or 1, for void or solid regions, respectively. For this work, $x_{\min}$ was set at 1e-6. This BESO formulation uses a material interpolation scheme:

$$\boldsymbol{E}(\boldsymbol{x_i}) = \boldsymbol{E}_1\boldsymbol{x_i^p} \tag{3}$$

where E_1 is the Young's modulus for the solid region, and p is the penalty exponent. As detailed in [22,23], and explained by Bendsoe and Sigmund [8], the sensitivity of the objective function with respect to the i^{th} element is

$$\frac{\partial \boldsymbol{C}}{\partial \boldsymbol{x_i}} = -\frac{\boldsymbol{p}\boldsymbol{x_i^{p-1}}}{2}\boldsymbol{u_i^T}\boldsymbol{k_i^0}\boldsymbol{u_i} \tag{4}$$

where k_i^0 denotes the stiffness matrix and u_i represents the displacement vector for the ith element. The relative ranking of the elemental sensitivities for both solid and void region elements can be expressed as

$$^{\boldsymbol{S}}\boldsymbol{\alpha_i} = \frac{-1}{\boldsymbol{p}}\frac{\partial \boldsymbol{C}}{\partial \boldsymbol{x_i}} = \begin{cases} \frac{1}{2}\boldsymbol{u_i^T}\boldsymbol{k_i^0}\boldsymbol{u_i} & \text{when } \boldsymbol{x_i} = 1 \\ \frac{\boldsymbol{x_{\min}^{p-1}}}{2}\boldsymbol{u_i^T}\boldsymbol{k_i^0}\boldsymbol{u_i} & \text{when } \boldsymbol{x_i} = \boldsymbol{x_{\min}} \end{cases} \tag{5}$$

where $^{S}\alpha_i$ is the structural sensitivity number for the i^{th} element. It can be seen that the sensitivity number for the solid region is equal to the elemental strain energy, and the sensitivity number for the void region is dependent on the value of p. For this work, p was selected to be 1, and therefore the structural sensitivity number was equal to the strain energy for both regions.

2.3. Heuristic sensitivity definition

Under a general optimization framework, one would ideally state the objective function in terms of the problem specific variables in order that the sensitivities of design variables can be easily obtained. However, in cases where doing this becomes challenging such as in the case of a coupled (structural + system) optimization,

Table 1
Parameters used for the coupled optimization.

Parameter	Description	Value
ω_1	Weights/parameters used for the weighted sum formulation of objective function	0.5
E_1	Young's modulus for the solid region	1
$x_{Structure}$	Material density used for structure	1
x_{Void}	Material density used for the void region	1e-6
x_{System}	Material density used for system	1e-3
P	Penalisation	1
v	Poisson's ratio	0.3
$R_{\min}$	Filter radius value used to avoid checker-boarding in topology optimisation	2
er	Evolution rate used for element removal in BESO	2%
V_f	Target volume fraction	40%
$Itr^{\lim it}$	Optimization iterations after which the process is terminated	80

one can attempt to solve the two problems as if they were overlaid. This necessitates the definition of appropriate sensitivities for each class of problem and their implementation in a combined objective function. As this work focuses on examples where the placement location of components is pre-determined/specified, the system associated elemental sensitivities can be determined exclusively from the routing aspect of system design using

$$^{R}\alpha_i = \frac{1}{1+d_i} \tag{6}$$

where, d_i is the distance (Euclidian measure) between the 'ith' element (within the discretized design domain) and the closest point from it on the routed paths. This assigns a lower value (between 0 and 1) for elements that are further away from a routed path and a value of '1′ to those elements which form a route.

The system elemental sensitivities can be combined with those of the structural counterpart using a weighted sum approach as shown in

$$^{C}\alpha_i = \omega_1 \times {}^{S}\alpha_i + (1-\omega_1) \times \left({}^{R}\alpha_i\right) \tag{7}$$

where, $^{S}\alpha_i$ represents the normalized (data range between 0 and 1) structural elemental sensitivities (i.e. strain energy densities) after thresholding the outliers (i.e. at point of loading and boundary conditions) and $^{R}\alpha_i$ represents the normalized system elemental sensitivities. $\omega_1 \in [0, 1]$ is a user defined weight to control the relative influence of the system design on the overall coupled solution.

Preliminary work by the authors [16] on coupling system design with TO considered the cantilever plate problem of Fig. 4. Four component locations (shown as circles) were identified using the resultant topology of a structure-only optimization (see Fig. 5e) so that the effect of the system inclusion on the resulting structure when employing a coupled optimization, can be investigated. A pair-wise routing between component locations utilizing the approximate routing method [9] (i.e. routes constrained to the medial axis of the structure) was considered for system design. The coupling employed the algorithm of Fig. 3 and utilized Eqs. (6) and (7) to assess solutions. Fig. 5 presents the effects of such a system integration when included in the process of TO. However, this implementation suffered from robustness issues arising from the unstable evolution (poor convergence) of the objective function during the iterative process of the optimization [16]. This was essentially due to the sudden changes in the skeletal topology resulting from any dis-connectivity in structural members. It is noteworthy that the skeletal topology governed the system configuration in the aforementioned work as the approximate routes were made to adhere to the skeletal topology. In this work, an improved coupling strategy is developed that addresses this problem and uses a more accurate routing method.

The two key advances made in this paper towards the coupled optimization algorithm of Fig. 3 are: i) an improved heuristic definition for system associated elemental sensitivities and ii) an improved method of combining the system elemental sensitivities

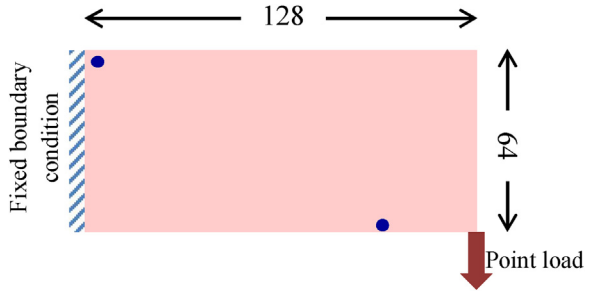

Fig. 6. The considered extruded 2D (2 voxel deep) cantilever problem.

with the structural sensitivities. For the former, the $^{R}\alpha_i$ values are 'bounded' to avoid unwanted influence in areas of the topology not pertinent to the routing, by setting $^{R}\alpha_i$ to zero for d_i greater than the filter radius or $R_{\min}$ (see Table 1).

$$^{R}\alpha_i = \frac{1}{1+d_i}(\text{bounded}) \tag{8}$$

and for the latter, an adaptive parameter λ defined as

$$\lambda = \frac{\sum {}^{S}\alpha_i}{\sum {}^{R}\alpha_i} \tag{9}$$

which is multiplied by $^{R}\alpha_i$ to ensure an appropriate contribution of the system associated elemental sensitivities towards the combined sensitivity, which is now defined as

$$^{C}\alpha_i = \omega_1 \times {}^{S}\alpha_i + (1-\omega_1) \times \left(\lambda \times {}^{R}\alpha_i\right) \tag{10}$$

Although, Eqs. (7) and (10) share the same weighted sum approach on the structure and system sensitivities that is necessary for the update of design variables, it is the improved formulation in the heuristics that the authors evaluate and discuss in the next section that results in a significant improvement on the previous formulation.

3. Simulations, results and discussion

This work raises two research questions which allow for an assessment of the appropriateness and robustness of the proposed coupling strategy.

Research question – I. What influence does the heuristic sensitivity definition (specifically, the use of $^{R}\alpha_i$(bounded) and λ) have on the coupled solution?

Research question – II. Whether it is advantageous to perform a coupled (structure + system) optimization or not? (As a comparative uncoupled solution, the authors refer to performing a TO to obtain a structure and subsequently adding the system design)

Each research question is best tackled with help of a test case. These test cases consider an extruded 2D cantilever problem as

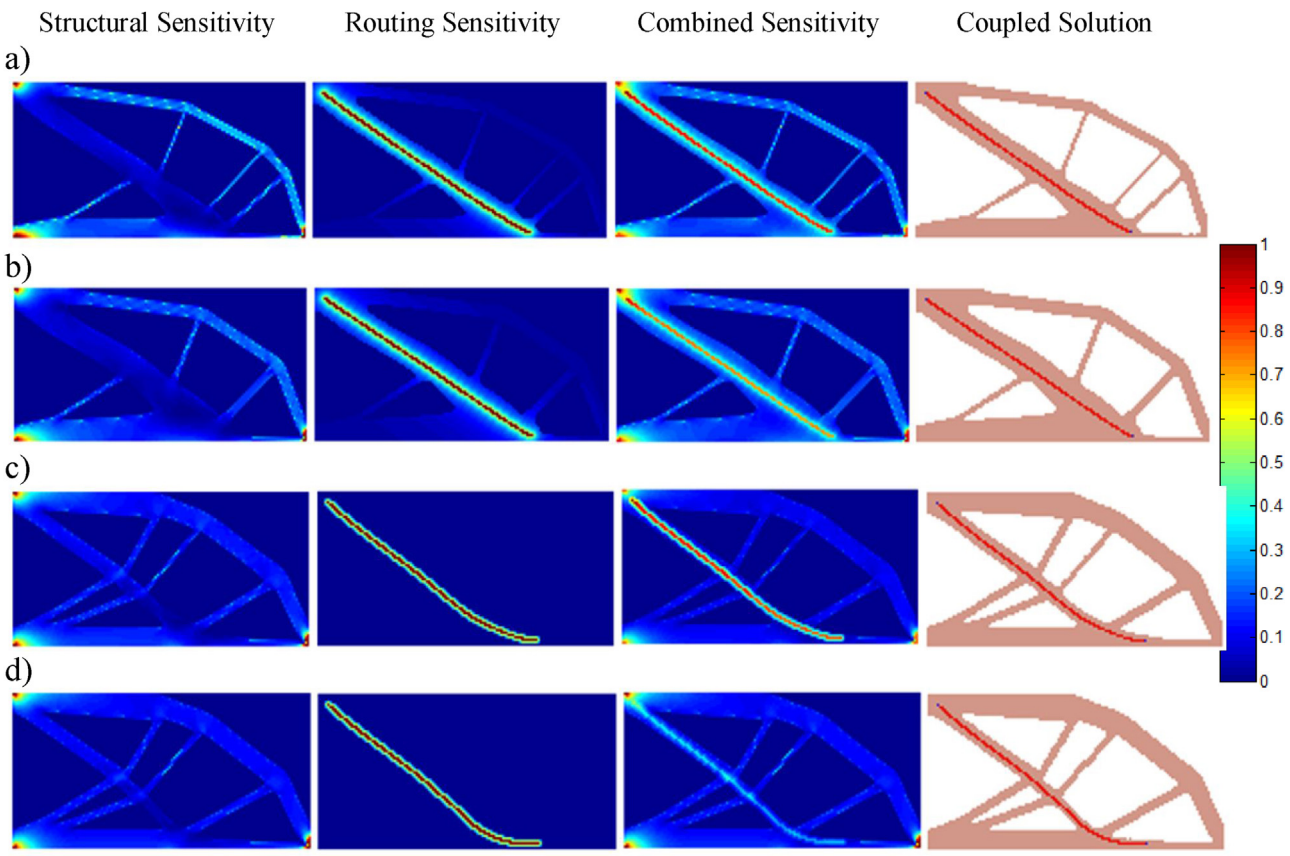

Fig. 7. Coupled optimization for a target V_f of 0.4 with a) ${}^{R}\boldsymbol{\alpha}_i$(unbounded) and λ (not included), b) ${}^{R}\boldsymbol{\alpha}_i$(unbounded) and λ (included), c) ${}^{R}\boldsymbol{\alpha}_i$(bounded) and λ (not included), d) ${}^{R}\boldsymbol{\alpha}_i$(bounded) and λ (included).

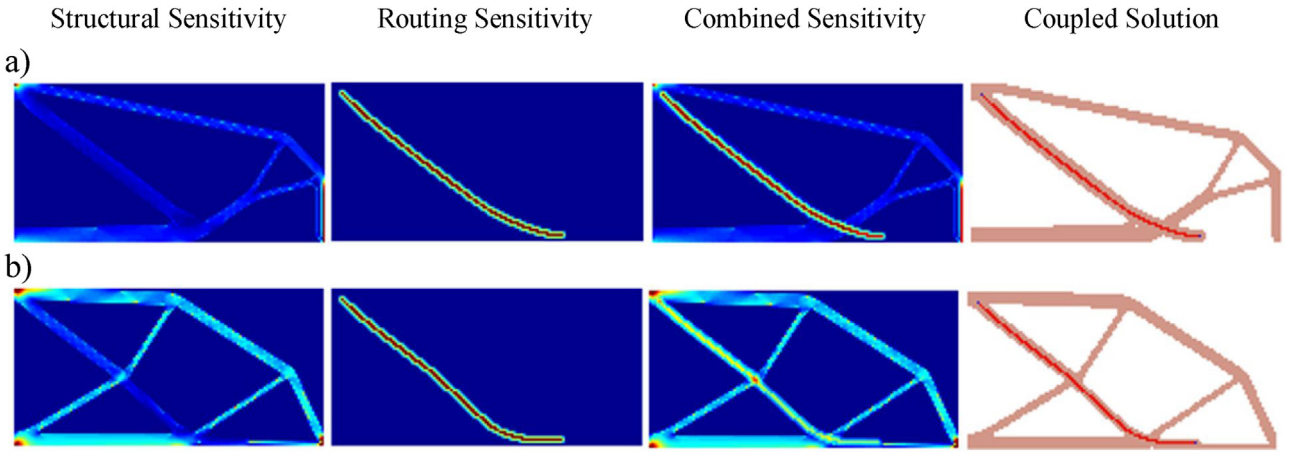

Fig. 8. Coupled optimization for a target V_f of 0.25 with a) ${}^{R}\boldsymbol{\alpha}_i$(bounded) and λ (not included), b) ${}^{R}\boldsymbol{\alpha}_i$(bounded) and λ (included).

shown in Fig. 6 (with the left edge fixed and a vertically downward force being applied to the bottom right corner). The extrusion extent of the design domain was kept to 2 voxels as this allowed for multiple routes to exist between components without overlaps. This is because routes are no longer limited to being planar and can exist in 3D. Two component locations (shown as circles) were identified using the resultant topology of a structure-only optimization so as to better understand the effect of the system inclusion on the resulting structure when employing a coupled optimization with the improved heuristics.

The parameters used to simulate the test cases are reported in Table 1. These include standard values for the material density of solid (structure) and void regions, specifically, 1 and a much lower value of 1e-6, respectively. An intermediate value was employed for the material density corresponding to the routing (system). This choice was made so that only a very weak contribution could be made by the finite elements representing the routes on the total strain energy of the structure (i.e. measure of structural stiffness) as the system is not intended to be load bearing for this study. Equal weighting was chosen for the objective function formulation as the focus of this study was not on investigating the influence of weighting parameter (ω_1). The elemental strain energies for this study were obtained by performing FEA using a commercial solver (MSc

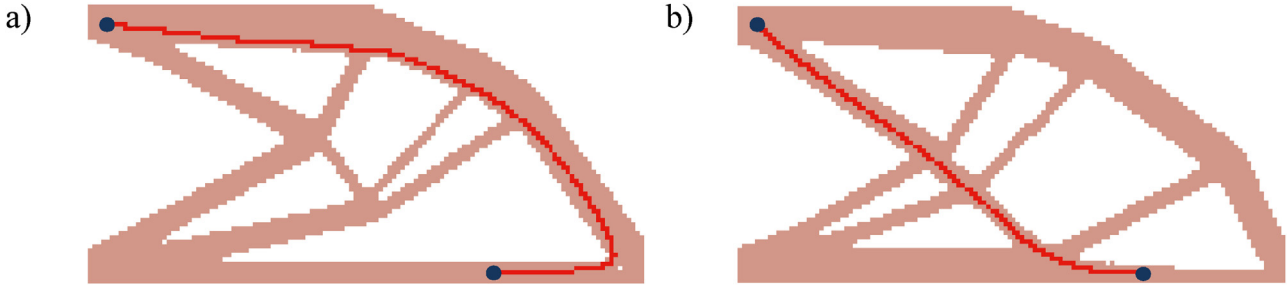

Fig. 9. Comparison in results for uncoupled and coupled optimization – a) routing performed on a (converged) topology optimized structure, b) routing performed as a coupled (structure + system) optimization problem.

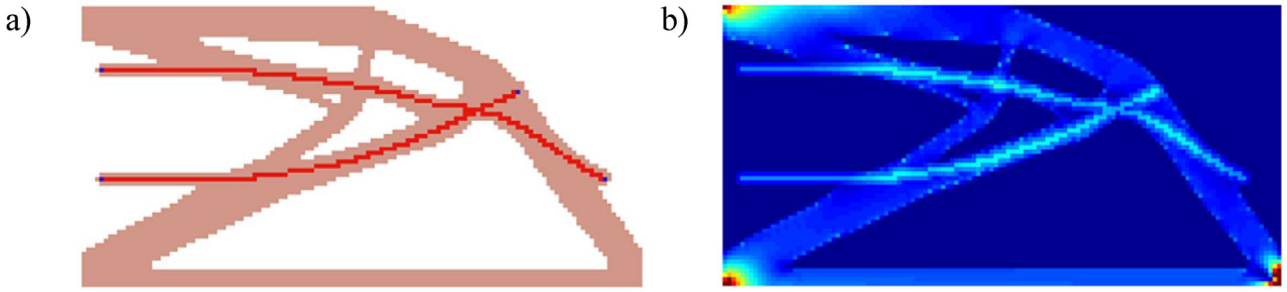

Fig. 10. Application to a more complex problem – a) coupled solution, b) combined sensitivity.

Nastran [37]) on a uniform mesh having an edge length of 1 unit (Fig. 6 shows the structure as 128 units by 64 units in dimension).

Results for the simulation of Test Case I (addressing research question I) are presented in Fig. 7. Here we analyse and attempt to understand the effect that ${}^{R}\alpha_i$(bounded) and λ have (independently) on the solution. Fig. 7a shows a characteristic straight-line route between the two placement locations, even when similar weighting for structure and system contributions (i.e. $\omega_1 = 0.5$) were used. This system dominated solution can be best understood by inspecting the combined sensitivities (${}^{C}\alpha_i$) of the voxels representing the route which in this case happens to acquire a nearly constant and notably higher value for the entire route. With a 50% weighting, this should not be the case as both the structure and system should contribute more or less equally towards the solution.

In Fig. 7b, with the inclusion of the adaptive parameter λ, a more balanced contribution of the system sensitivities towards the combined sensitivities is achieved. This is evident from the variability in combined sensitivity values for the voxels comprising the route. However, even in this case a characteristic straight-line route is obtained for the final solution, indicating a clear dominance of the system sensitivity towards the combined sensitivity. This is due to ${}^{R}\alpha_i$ being unbounded, resulting in an unnecessarily large region of influence over which the system sensitivities play a role, which makes the structure near the routes unnecessarily bulky. This system sensitivity dominance makes the possibility of element removal near the route very low, causing the system solution to have no noticeable change with the optimization iterations.

Conversely, a more intuitive solution where the system and structure seem to evolve competing with each other can be seen in Fig. 7c-d where the values of ${}^{R}\alpha_i$are bounded. However, only marginal differences can be seen when comparing the voxels representing the routes in the coupled solutions of Fig. 7c and d. This can be attributed to the relatively high structural volume compared to the system volume, making the effect of λ (in Fig. 7d) less noticeable. To test this hypothesis further, another coupled optimization was performed but this time the target V_f was set as 0.25 instead of the previously used value of 0.4.

Table 2
Comparison in structural performance between solutions of Fig. 8 (with and without the inclusion of λ).

	Fig. 8a (λ – not included)	Fig. 8b (λ – included)	difference
Total Strain Energy	88.2	67.4	23.6%

Table 3
Comparison in performance between uncoupled and coupled optimization.

	Uncoupled solution	Coupled solution	difference
Path length (pixels)	196	138	30%
Total Strain Energy	39.9	40.2	< 1%
Max. displacement (pixels)	76.7	77.4	< 1%

With the lower value for the ratio of structure to system volume in the solution of Fig. 8 (where the coupled optimization problem is performed for a target V_f of 0.25) as compared to that in the case of target $V_f = 0.4$, a more notable influence of λ can be seen – both the resulting topology of the structure and the pixels comprising the route are seen to develop during the optimization with the improved heuristics. It is common for solutions to get trapped in local minima in a non-convex problem space, such as that seen in discrete SIMP or BESO. As a consequence, the evolution of the solution is history dependent, the different contributions from routing sensitivities (i.e. with or without the incorporation of λ) play a dominant role. This is supported by the 23.6% difference in total strain energy values (a measure for compliance or inverse of global stiffness) observed for the solutions of Fig. 8 a and b (values reported in Table 2). Moreover, it is clearly evident from the well-distributed and smoothly transitioning values for the combined sensitivities in Fig. 8b that: i) having ${}^{R}\alpha_i$ bounded, and ii) the inclusion of the adaptive parameter λ, is necessary to obtain a reliable solution as only then can one ensure the appropriate contribution of the system sensitivities towards the combined sensitivities for a multifunctional problem.

Results for the simulation of Test Case II addressing research question II (i.e. whether to perform (structure + system) coupled optimization or not?) are shown qualitatively as Fig. 9 and pre-

sented quantitatively in Table 3. The pixels comprising the route are very dissimilar for coupled and uncoupled solutions and this is to be expected as the system design is constrained to the final topology of the structure in the uncoupled problem. By adopting a coupled problem formulation, nearly 30% reduction in path length is achieved. Importantly, despite the visual differences in structural topology, negligible difference (< 1%) in the values for total strain energy is observed. From the considered example, it can be inferred that the system design benefits under a coupled optimization formulation whilst having little effect on the structural performance.

To gain a better assessment of the effects of coupling on the structural performance, a more complex routing scenario was considered where two component pairs are chosen such that the placement locations lie outside the resulting structure when one considers the topology optimized geometry of an uncoupled problem (specifically, topology of Fig. 9a). Fig. 10a shows how the structural topology has evolved to accommodate these routes joining the two component pairs in case of a coupled optimization. From a purely structural performance stand-point, the topology of Fig. 10a has 15% higher total strain energy (i.e. less stiff) as compared to that of Fig. 9a. However, it must be noted that the latter has undergone a single-objective optimization (where only strain energy or inverse of stiffness was minimised) whilst the former has been subjected to the coupled optimization where a weighted sum approach is considered for optimization. Such a coupling, in principle, should ensure the best material layout along-side optimal system configuration (in this work – shortest routes). This is because the routing between the components can't be realized on the structural topology of Fig. 9a for the specified placement locations.

The proposed coupling method has shown promise when tackling MFAM problem and as the capability of the system design employed for this work has already been demonstrated for 3D applications [9], one can consider this strategy with confidence (in its native form or by extending it further by applying to different classes of problem and/or different optimization algorithms) to solve similar (structure + system) coupled problems in 3D. It must be noted that this method caters for the multiple objectives via a single weighted sum approach and consequently will suffer from the limitations of this formulation. Where weighted sum approaches may prove to be inadequate, a more generic multi-objective consideration such as the pareto-front criterion can be considered.

4. Concluding remarks

This paper has presented a coupled optimization formulation which allows for the optimal material and system lay-out to be identified as it tackles a system design problem overlaid on a structural design problem. Although, the immediate application for this development is enabling the design of additively manufactured (jetted) multi-material parts with embedded functional systems, for example a structural part with electrical componentry and conductive tracks, nevertheless, the strategy presented herein should be considered for tackling a more general class of engineering problems. For instance, civil engineering structures (buildings/bridges) that incorporate systems (pipes/cables). This coupled optimization development marks a significant step towards being able to exploit the design freedom offered by MMAM.

The main contribution of this paper is the improved heuristic definition that allows for a more appropriate coupling strategy, where the system design is performed concurrently with the structural optimization. This is achieved by accommodating the effects of system incorporation on the structural response of the part at every iteration within a modified bidirectional evolutionary structural optimization.

The simulation results for the evaluated extruded 2D cantilever test cases show the suitability of the proposed coupling method where the system sensitivities, specifically routing sensitivities, are combined with the structural sensitivities for a multifunctional design problem. The authors believe this contribution will provide the necessary design-innovation and in-turn the manufacturing incentive to realize multifunctional AM or MFAM products.

Acknowledgment

This work was supported by the Engineering and Physical Sciences Research Council [grant number EP/I033335/2].

References

[1] E. MacDonald, R. Wicker, Multiprocess 3D printing for increasing component functionality, Science 353 (6307) (2016) (p. aaf2093-aaf2093).
[2] A.J. Lopes, E. MacDonald, R.B. Wicker, Integrating stereolithography and direct print technologies for 3D structural electronics fabrication, Rapid Prototyp. J. 18 (2) (2012) 129–143.
[3] J. Vaithilingam, E. Saleh, C. Tuck, R. Wildman, I. Ashcroft, R. Hague, P. Dickens, 3D-inkjet printing of flexible and stretchable electronics, Proceedings of the 26th Solid Freeform Fabrication Symposium (2015).
[4] E. Saleh, J. Vaithilingam, C. Tuck, R. Wildman, I. Ashcroft, R. Hague, P. Dickens, 3D inkjet printing of conductive structures using in-situ IR sintering, Proceedings of the 26th Solid Freeform Fabrication Symposium (2015).
[5] S.-P. Chen, H.-L. Chiu, P.-H. Wang, Y.-C. Liao, Inkjet printed conductive tracks for printed electronics, ECS J. Solid State Sci. Technol. 4 (4) (2015) P3026–P3033.
[6] K. Vidimce, S.-P. Wang, J. Ragan-Kelley, W. Matusik, OpenFab: a programmable pipeline for multi-Material fabrication, ACM Trans. Graphics 32 (4) (2013) 1–11.
[7] R. Ponche, J.Y. Hascoet, O. Kerbrat, P. Mognol, A new global approach to design for additive manufacturing, Virtual Phys. Prototyp. 7 (June (2)) (2012) 93–105.
[8] M.P. Bendsoe, O. Sigmund, Topology Optimization: Theory, Methods and Applications, Springer, 2003.
[9] A. Panesar, D. Brackett, I. Ashcroft, R. Wildman, R. Hague, Design framework for multifunctional additive manufacturing: placement and routing of 3D printed circuit volumes, J. Mech. Des. 137 (11) (2015).
[10] J. Zhu, W. Zhang, P. Beckers, Integrated layout design of multi-component system, Int. J. Numer. Methods Eng. 78 (2009) 631–651.
[11] J.H. Zhu, W.H. Zhang, Integrated layout design of supports and structures, Comput. Methods Appl. Mech. Eng. 12 (Jan) (2010) 557–569.
[12] W. Zhang, L. Xia, J. Zhu, Q. Zhang, Some recent advances in the integrated layout design of multicomponent systems, J. Mech. Des. 133 (10) (2011) 104503.
[13] T. Buhl, Simultaneous topology optimization of structure and supports, Struct. Multidiscip. Optim. 23 (5) (2002) 336–346.
[14] E. Beyne, 3D system integration technologies, International Symposium on VLSI Technology, Systems, and Applications (2006) 1–9.
[15] A. Panesar, D. Brackett, I. Ashcroft, R. Wildman, R. Hague, Design optimization strategy for multifunctional 3D printing, 25th Interational Solid Freeform Fabrication Symposium (2014) 592–605.
[16] A. Panesar, D. Brackett, I. Ashcroft, R. Wildman, R. Hague, Design optimization for multifunctional 3D printed structures with embedded functional systems, 11th World Congress on Structural and Multidisciplinary Optimisation (2015).
[17] N. Abboud, M. Grötschel, T. Koch, Mathematical methods for physical layout of printed circuit boards: an overview, OR Spectr. 30 (May (3)) (2007) 453–468.
[18] T.F. Chan, J. Cong, J.R. Shinnerl, K. Sze, M. Xie, Multiscale Optimization in VLSI Physical Design Automation, Multiscale Optimization Methods and Applications (Nonconvex Optimization and Its Applications), vol. 82, Springer-Verlag, 2006, pp. 1–67.
[19] S. Areibi, Z. Yang, Effective memetic algorithms for VLSI design = Genetic algorithms + local search + multi-level clustering, Evol. Comput. 12 (Jan (3)) (2004) 327–353.
[20] J.-H. Park, R.L. Storch, Pipe-routing algorithm development: case study of a ship engine room design, Expert Syst. Appl. 23 (Oct (3)) (2002) 299–309.
[21] X. Ma, K. Iida, M. Xie, J. Nishino, T. Odaka, H. Ogura, A genetic algorithm for the optimization of cable routing, Systems Comput. Jpn. 37 (Jun (7)) (2006) 61–71.
[22] G.I.F. Thantulage, Ant Colony Optimization Based Simulation of 3D Automatic Hose/pipe Routing. PhD, Brunel University, 2009.
[23] C. Velden, C. Bil, X. Yu, A. Smith, An intelligent system for automatic layout routing in aerospace design, Innovations Syst. Software Eng. 3 (May (2)) (2007) 117–128.
[24] H.Y. Guo, L. Zhang, L.L. Zhang, J.X. Zhou, Optimal placement of sensors for structural health monitoring using improved genetic algorithms, Smart Mater. Struct. 13 (Jun (3)) (2004) 528–534.

[25] E.B. Flynn, M.D. Todd, A Bayesian approach to optimal sensor placement for structural health monitoring with application to active sensing, Mech. Syst. Sig. Process. 24 (May (4)) (2010) 891–903.
[26] T. Lee, R. Kashyap, C. Chu, Building skeleton models via 3-D medial surface/axis thinning algorithms, Graphical Models Image Process. 56 (6) (1994) 462–478.
[27] M. Kerschnitzki, P. Kollmannsberger, M. Burghammer, G.N. Duda, R. Weinkamer, W. Wagermaier, P. Fratzl, Architecture of the osteocyte network correlates with bone material quality, J. Bone Miner. Res. 28 (8) (2013) 1837–1845.
[28] E.W. Dijkstra, A note on two problems in connexion with graphs, Numerische Math. 1 (1959) 269–271.
[29] G. Peyre, FM Code, 2009. [Online]. Available: http://www.mathworks.co.uk/matlabcentral/fileexchange/6110-toolbox-fast-marching.
[30] X. Huang, Y.M. Xie, Evolutionary Topology Optimization of Continuum Structures, first ed., Wiley Publication, 2010.
[31] M.Y. Wang, X. Wang, D. Guo, A level set method for structural topology optimization, Comput. Methods Appl. Mech. Eng. 2 (2003) 227–246.
[32] O. Sigmund, Design of multiphysics actuators using topology optimization – Part I: One material structures, Comput. Methods Appl. Mech. Eng. 190 (2001) 6577–6604.
[33] E. Hassan, Metallic Antenna Design Based on Topology Optimization Techniques, 2013.
[34] X. Huang, Y.M. Xie, Bi-directional evolutionary topology optimization of continuum structures with one or multiple materials, Comput. Mech. 43 (July (3)) (2008) 393–401.
[35] X. Huang, Y.M. Xie, A further review of ESO type methods for topology optimization, Struct. Multidiscip. Optim. 41 (Mar (5)) (2010) 671–683.
[36] O. Sigmund, K. Maute, Topology optimization approaches: a comparative review, Struct. Multidiscip. Optim. 48 (2013) 1031–1055.
[37] M.S.C. Nastran, MSC Software Corporation, California USA, 2014.